ELSEVIER

Journal of Molecular Catalysis A: Chemical 155 (2000) 143–153

JOURNAL OF MOLECULAR CATALYSIS A: CHEMICAL

www.elsevier.com/locate/molcata

Control of bandgap of iron oxide through its encapsulation into SiO_2-based mesoporous materials

Masakazu Iwamoto *, Takayuki Abe, Yukio Tachibana

Catalysis Research Center, Hokkaido University, Sapporo 060-0811, Japan

Received 30 January 1999; accepted 16 June 1999

Abstract

Nanoparticles of iron oxide were encapsulated into the pores of Si-MCM-41 and porous vycor glass (PVG) with pore diameters 2.1–4.5 nm. Transmission electron micrographs (TEM) observation has revealed the formation of iron oxide particles in the pores after an adequate preparation including a suspension treatment in water. Ultraviolet–visible absorption spectra (UV-VIS) of iron oxide loaded on the respective supports were greatly changed with the pore diameters. The bandgaps of iron oxide, evaluated from the absorption edges of the UV-VIS spectra, were significantly widened with decrease in the pore diameters. The dependence of the bandgap on the pore diameter could well be explained by the Brus' equation when the effective mass of an electron and a hole in iron oxide was assumed to be 0.27. It follows that the bandgap was changed by the quantum size effect and could be controlled by the pore size of support.

Keywords: Bandgap; Iron oxide; Porous vycor glass

1. Introduction

Nanometer-sized semiconductor particles have attracted much attention because of interest in their unique size-dependent optical properties such as absorption spectra and third-order nonlinearity [1,2]. Although there are many approaches to prepare the nanoparticles in solution [3], glasses [4], and polymers [5], two kinds of major problems have remained to be solved. The first is how to prepare the nanoparticles with a uniform size. The second significant problem is how to maintain the properties of the resulting nanoparticles. Recently, zeolites have been used as cages and stabilizers for well-defined semiconductor particles from this viewpoint. Typical examples are the loading of GaP and CdS in Y-type or ultrastable Y-type zeolites [6]. The use of zeolite matrixes has been revealed to be an effective method for the preparation of ultrasmall particles but their very small pore sizes [7] resulted in several limitations such as too large bandgaps and instability of the particles.

Several years ago, a new family of mesoporous materials, designated MCM-41 (abbreviated as M41), have been developed by using liquid crystal templates [8–10]. M41 is a silica-based mesoporous material with a regular hexagonal array of uniform pores. The diameter of pores can be controlled from 2 to 10 nm by

* Corresponding author. Tel.: +81-11-706-2907; fax: +81-11-757-8126.

1381-1169/00/$ - see front matter
PII: S1381-1169(99)00330-1

change in the alkyl chain length of the surfactant used or by further addition of organic molecules such as 1,3,5-trimethylbenzene [8] because the surfactants and organic molecules form rod-like micelles and act as the templates for the pore formation. Many studies on its potential applications for catalysts [11–13], molecular sieves [14,15], and adsorbents have widely been conducted so far. Only a few investigators [16–20] have tried the use of M41 as molds for preparation of nanoparticles. Although TiO_2, Au, GaAs, and InP have been attempted to be supported in the pores of M41 in these studies, the formation of large particles are observed at the outside of the mesopores as well as the formation of nanoparticles in the pores.

In our preliminary report [17], we have shown that the nanoparticles of iron oxide could be encapsulated into the 2.2-nm pores of M41 and the bandgap of the resulting iron oxide particles was widened from 2.1 to 4.1 eV owing to the quantum size effect. In this study, two kinds of M41 and three kinds of porous vycor glass (PVG) with a variety of pore sizes have been used as the molds for the formation of iron oxide particles. It will be shown that the bandgaps of the iron oxide supported in the silica-based mesoporous materials are greatly widened depending on the pore sizes and the dependency can be explained by the quantum size effect. The present results would provide firstly a novel technique to control the bandgap of semiconductor without any additive or any formation of junction and secondly a new method to evaluate the effective mass of semiconductors. The resulting materials would be interesting in the field of catalysis and photocatalysis.

2. Experimental

2.1. Materials

Colloidal silica (Snowtex-20) obtained from Nissan Chemical was used as the silica source for the synthesis of M41 and dodecyltrimethylammonium (C_{12}TMA) chloride or cetyltrimethylammonium (C_{16}TMA) chloride obtained from Kanto Kagaku was employed as the surfactant. M41 was synthesized from the mixture with the composition 1.0 SiO_2:0.7 C_{12}TMA or C_{16}TMA chloride: 0.24 NaOH:54.9 H_2O. The mixture was loaded into a Teflon bottle in an autoclave after being homogenized at room temperature by stirring, and statically heated at 403 K for 48 h. The resulting as-synthesized solid product (M41) was filtered and suspended in deionized water at 353 K for 20 h. The washed M41 was filtered again and dried at 353 K. Finally, it was calcined at 873 K for 6 h to yield the pure silica M41. The M41s prepared by using C_{12}TMA and C_{16}TMA were denoted M41-12 and M41-16, respectively.

PVG was purchased from Corning Glass Works and treated with a nitric acid solution and a 30% H_2O_2 solution at room temperature and then calcined at 973 K for 3 h to remove inorganic and organic impurities on the surface before the use (pretreatment). The pore size of the pretreated sample was controlled by heating at 1263 or 1273 K in air for 3 h because it has widely been reported that the calcination of PVG at high temperature resulted in shrinking of the pores. The PVG samples obtained were denoted PVG-1263 and -1273, respectively. The parent PVG sample pretreated was abbreviated as PVG-N.

2.2. Loading of iron oxide in the pores of supports

The loading of iron oxide nanoparticles on various supports was carried out by the incipient wetness method with 0.04 M aqueous iron(II) nitrate solution at pH 2.3. After being dried under vacuum, the resulting products were suspended in deionized water at room temperature for 1 h and dried at 353 K (suspension treatment). Finally, samples were heated at a heating rate of 10 K/min and calcined at 973 K for 3 h

Table 1
Properties of the supports and the Fe/supports

Sample	Iron oxide loaded[a] (wt.%)	$d(100)$[b] (nm)	Surface Area[c] ($m^2\ g^{-1}$)	Pore volume[c] ($cm^3\ g^{-1}$)	Pore diameter[c] (nm)	Bandgap[d] (E) (eV)
M41-12	–	3.416	1028	0.749	2.24	–
M41-16	–	3.962	1018	1.320	2.65	–
PVG-1273	–	–	16	0.041	3.91	–
PVG-1263	–	–	46	0.093	3.92	–
PVG-N	–	–	205	0.302	4.45	–
Fe/M41-12	0.61	3.349	994	0.713	2.13	4.20
Fe/M41-16	0.59	3.879	999	1.150	2.50	4.06
Fe/PVG-1273	0.05	–	18	0.048	3.90	3.71
Fe/PVG-1263	0.13	–	44	0.091	3.92	2.71
Fe/PVG-N	0.41	–	189	0.275	4.45	2.46
Bulk Fe_2O_3						2.14

[a] Calculated as Fe_2O_3.
[b] Determined by XRD for the hexagonal structure of the mesoporous materials.
[c] Measured through a N_2 adsorption/desorption technique.
[d] Evaluated from the respective UV-VIS spectra on the assumption of the direct interband transition.

in air. The samples prepared were denoted Fe/supports. The Fe contents were measured by an inductively coupled plasma analysis (ICP) spectroscopy as described in the later section and shown in Table 1.

In the above treatment, the suspension treatment is indispensable for migration of Fe ions loaded on the outer surface into the pores, as will be reported in Section 3. Without the suspension treatment, the formation of iron oxide particles was confirmed to proceed not only in the pores but also on the outer surface of M41. Although the details of the reactions occurring during the suspension treatment are not clarified yet, the above treatment has been employed in every preparation of Fe/supports.

2.3. Characterization

X-ray powder diffraction (XRD) data were obtained on a MAC Science MXP3 using Cu K_α radiation. The scanning was performed from 1° to 10° (2θ) in units of 0.004° with a counting time of 1 s at each step. Transmission electron micrographs (TEM) were collected on a JEOL JEM-1200EXII with acceleration voltage of 120 kV or a Hitachi H-1250 M of 1000 kV. Nitrogen adsorption/desorption isotherms were obtained at 77 K on a Quanta Chrome Autosorb-1. The pore size distributions were evaluated from the respective desorption isotherms by using the BJH method and the surface areas were determined by the BET method. Elemental analyses of samples were performed by the ICP on a Perkin Elmer Optima 3000 after the samples were dissolved into HF aqueous solutions. Diffuse reflectance ultraviolet-visible absorption spectra (UV-VIS) were measured on a Shimadzu 2100 spectrophotometer.

3. Results and discussion

3.1. Effect of the suspension treatment during the preparation

We first attempted to directly observe the particles of iron oxide incorporated into the pores of M41 by TEM (JEOL JEM-1200EXII). No image of iron oxide nanoparticles, however, could be observed, probably owing to the little contrast between the pore spaces and the nanoparticles of iron oxide. In order to confirm the presence of iron oxide nanoparticles in the pores of M41, therefore, Pt was loaded on iron oxide particles by a photodeposition technique

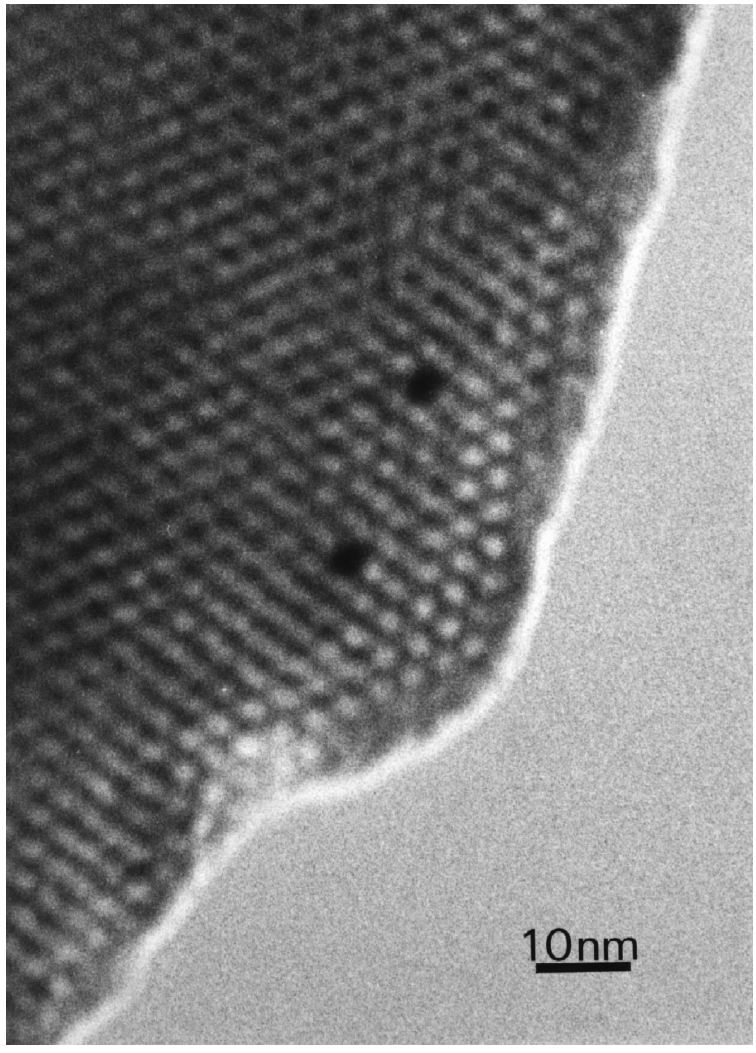

Fig. 1. TEM image of the Pt-loaded Fe-M41-12. It was taken at the magnification of 1,620,000 and the bar in the figure shows 10 nm.

in a $PtCl_6^{2-}$ solution.[1] It was confirmed in separate experiments that the photodeposition of Pt takes place on the bulk Fe_2O_3[2] and not on the parent M41. Fig. 1 shows a typical top view of the Pt-loaded Fe/M41-12. In the center of the image, two black spots assignable to thin Pt films deposited on the surface of the iron oxide nanoparticles can clearly be observed. The sizes of the Pt-covered particles in the pores were uniform but their diameters could not be determined exactly since the sizes changed during the observation of the TEM images.[3] It is clear that the sizes did not exceed the sum of the pore diameter and the wall thickness. In the pho-

[1] The photodeposition of Pt was carried out in a 0.01 mol dm^{-3} $H_2PtCl_6 + 1\%(m/m)$ MeOH solution for 30 min using a 400 W high pressure mercury lamp. The detailed method of the Pt photodeposition on TiO_2 was described in Ref. [21,22].

[2] The bulk Fe_2O_3 sample was prepared by the thermal decomposition of iron (III) nitrate at 973 K for 3 h in air.

[3] The change in the diameters of the Pt particles were due to the migration of the Pt atoms or the charging effect caused by the irradiation with the electron beam.

tographs of the side view of the Pt-loaded Fe/M41-12, most of the nanoparticles were distributed within ca. 100 nm from the entrance of pores.

It should be noted that no Pt particles existed on the outer surface of M41-12 after the suspension treatment. In contrast, on Fe/M41-12 prepared without the treatment, not only the particles in the pores but much bigger Pt-covered particles on the outer surface of M41-12 were observed. The amounts of iron oxide loaded before and after the suspension treatment were 0.62 and 0.61 wt.%, respectively, indicating that the treatment did not cause any change in the amount of iron oxide loaded. It follows that the suspension treatment during the preparation would promote migration of iron ions loaded on the outer surface into the pores.

The UV-VIS absorption spectra of Fe/M41-12 with and without the suspension treatment, calculated by using the Kubelka–Munk function [$F(R_\infty)$], are shown in Fig. 2(B) and (C), respectively. The absorption spectra of bulk Fe_2O_3 sample and M41-12 are also depicted as (A) and (D), respectively. The parent M41-12 gave little absorption in the range 240–800 nm . With the bulk Fe_2O_3, the direct and indirect interband transitions were observed at ca. 500 and 670 nm, respectively. In the absorption spectrum of Fe/M41-12 without the suspension treatment (spectrum b), one peak at ca. 250 nm and two shoulders at ca. 370 and 510 nm were shown. In contrast to these spectra, Fe/M41-12 with the suspension treatment yielded only one absorption band at ca. 250 nm. Taking the TEM observation into consideration, the bands at 370 and 510 nm are attributable to the transition in the bulk Fe_2O_3 particles on the outer surface of M41-12, while the band at 250 nm can be assigned to that in the iron oxide nanoparticles in the pores. On the basis of the above TEM and UV-VIS observation, one can conclude that the suspension treatment during the preparation of Fe/supports is indispensable to selectively

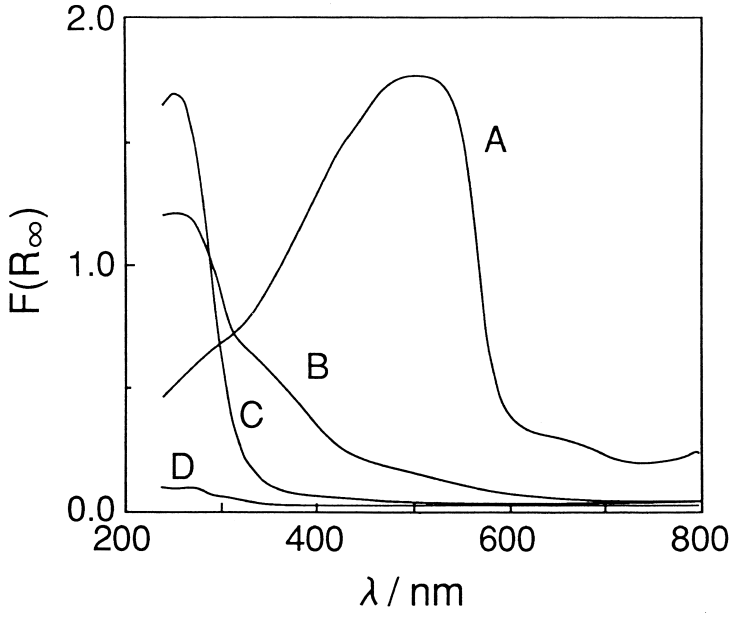

Fig. 2. Diffuse-reflectance UV-VIS spectra of (A) bulk Fe_2O_3, (B) Fe/M41-12 without the suspension treatment during the preparation, (C) Fe/M41-12 with the suspension treatment, and (D) parent M41-12. All reflectance spectra were converted to respective absorption spectra by using the Kubelka–Munk function. The reference was $BaSO_4$.

support iron oxide particles in the pores. The reaction or phenomenon during the treatment has remained unclear.

3.2. Characteristics of the Fe / supports

XRD analysis was carried out to determine the structure of the M41 materials. In the XRD patterns of the parent M41s, depicted in Fig. 3, three clear peaks and one very weak peak were observed and assignable to (100), (110), (200), and (210), respectively, indexed on a hexagonal unit cell. The first intense (100) peaks of M41-12 at $2\theta = 2.58°$ and of M41-16 at 2.23° correspond to the *d*-spacing of 3.42 and 3.96 nm, respectively. The XRD patterns of Fe/M41 samples were essentially the same as those of the parent M41 samples, but all the peaks were slightly shifted to higher 2θ by ca. 0.05°. The results indicate that the hexagonal structure of M41 was maintained throughout the incorporation treatment of iron oxide, and that the lattice structure of M41 was slightly shrunken by the supporting treatment by 0.07–0.08 nm. When the parent M41 samples were calcined at 973 K for 3 h in air, the XRD patterns also shifted to higher 2θ by ca. 0.04°. At the moment, the shift of the XRD peaks of the Fe/M41 samples cannot be fully interpreted by the heating effect alone.

Each XRD pattern of the parent PVG or the Fe/PVG sample gave only a broad peak at ca. $2\theta = 25°$. This is due to the amorphous structure of the supports. It should be noted that no XRD peak attributable to any kind of iron oxide was observed on the Fe/M41 and Fe/PVG samples, indicating no formation of large crystalline particles of iron oxide.

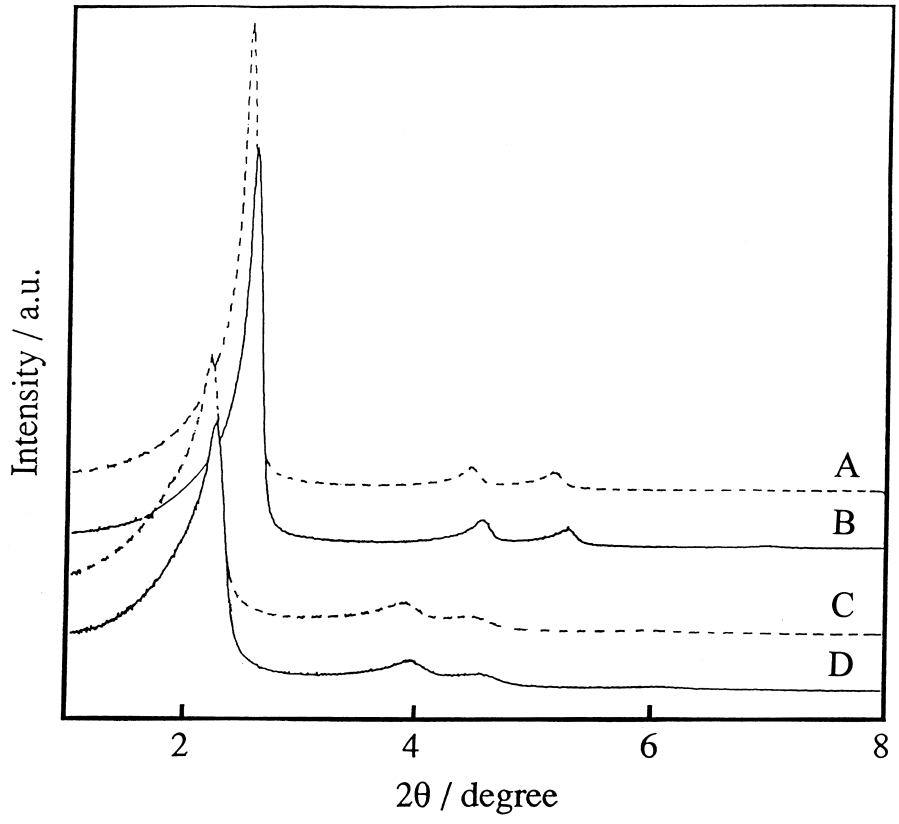

Fig. 3. XRD profiles of (A) M41-12, (B) Fe/M41-12, (C) M41-16, and (D) Fe/M41-16.

The pore diameters and the BET surface areas of the samples were determined by N_2 adsorption/desorption isotherms. Fig. 4 shows the pore distributions, calculated by using the respective desorption isotherms and a BJH method, of the Fe/support samples. It is clear that the distributions of pores are sufficiently narrow on all samples. In addition, the pore diameters are dependent on the chain length of surfactant used in the preparation of M41 or the calcination temperature of the PVG samples, as has already been reported by many workers. The pore diameters, the pore volumes, and the BET surface areas of the Fe/supports have

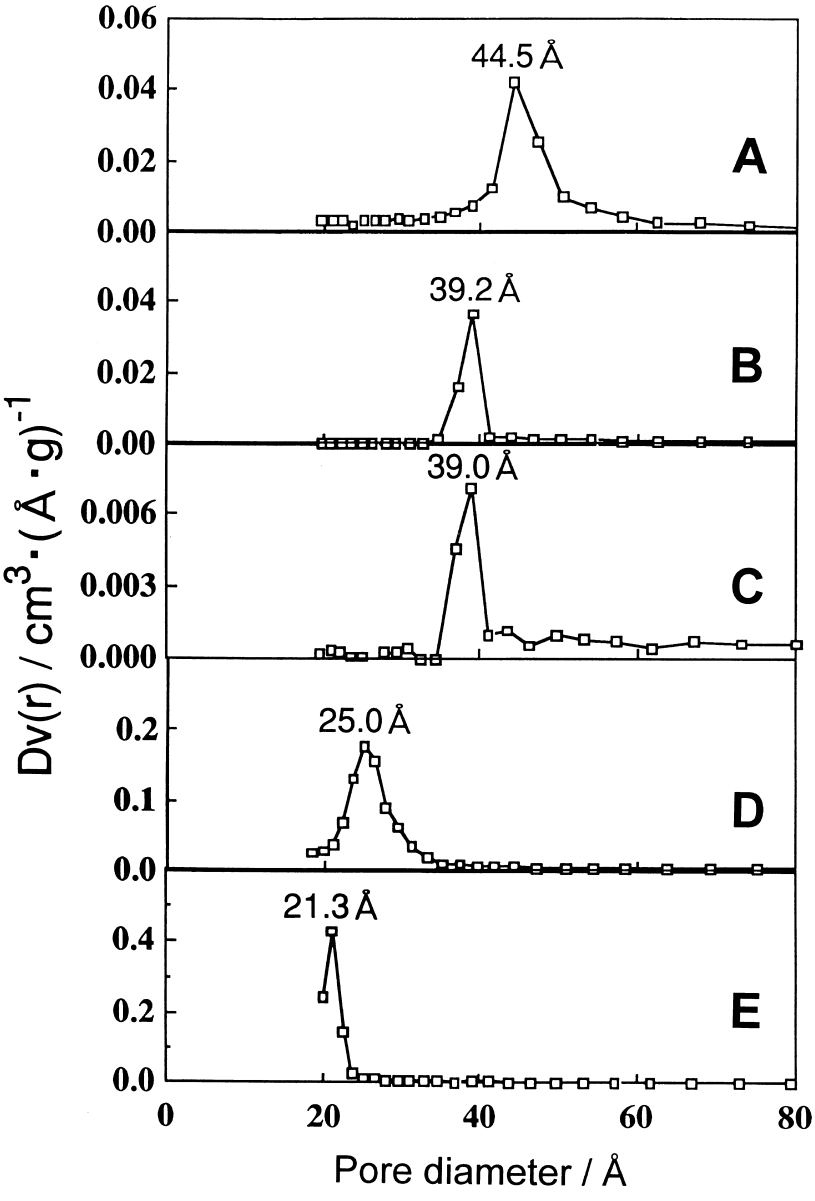

Fig. 4. Pore size distributions, determined by N_2 desorption isotherms at 77 K, of (A) Fe/PVG-N, (B) Fe/PVG-1263, (C) Fe/PVG-1273, (D) Fe/M41-16, and (E) Fe/M41-16. The data were obtained after the calcination at 973 K for 3 h.

been summarized in Table 1 together with those of the supports. Although the pore diameters of the PVG samples did not change with the supporting treatment of iron oxide, those of the M41-12 and -16 samples slightly decreased from 2.24 and 2.65 nm to 2.13 and 2.50 nm, respectively. The slight change in the lattice structure has also been demonstrated by the XRD analyses, though the decrements in 0.11 and 0.15 nm evaluated from the N_2 adsorption are not identified with those (0.07–0.08 nm) determined by XRD. The loading treatment of iron oxide would result in the decrease of pore size, in shrinking of the lattice of M41, or in increase in the wall thickness; the reasons should be clarified in the near future.

In the previous section, the TEM observation of the particles loaded has clarified their presence at the inside of pores after the treatment of Pt photodeposition. The precise sizes of the

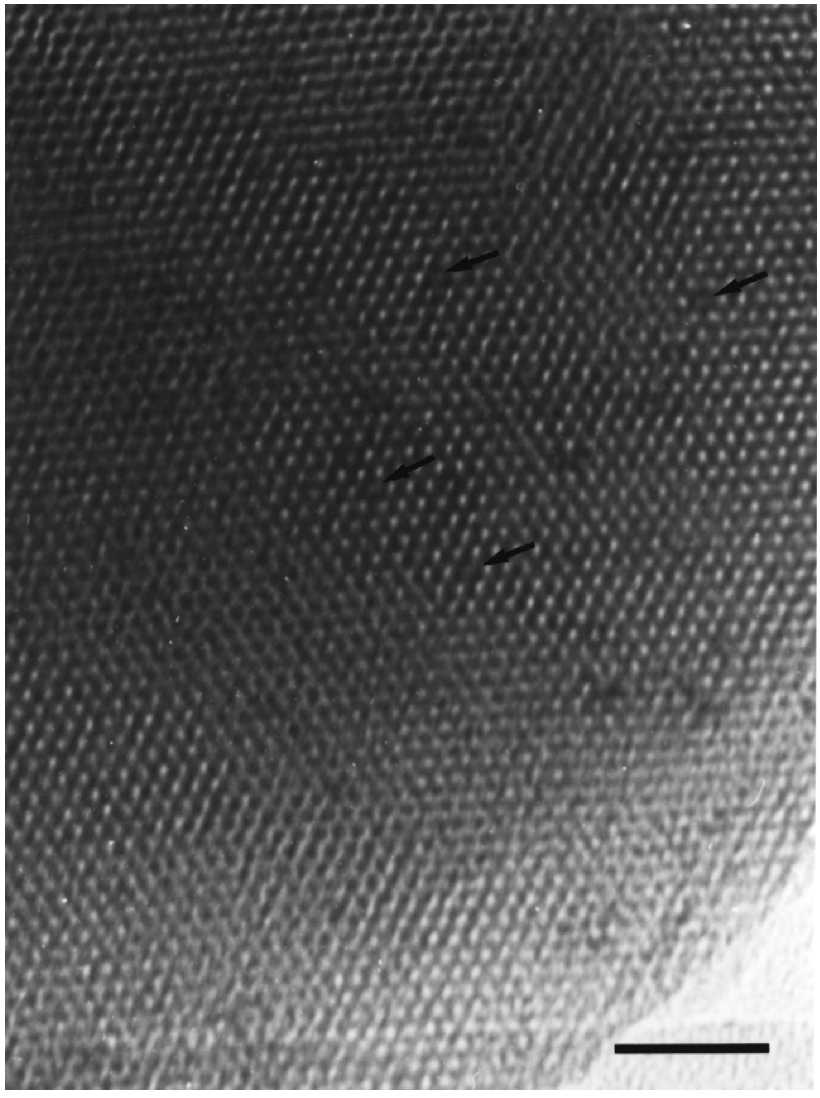

Fig. 5. TEM image of Fe/M41-12 observed on Hitachi H-1250M with acceleration voltage of 1000 kV. The arrows indicate presence of iron oxide particles in the pores of the support and the bar in the figure shows 30 nm.

particles, however, were unclear because the darkness of the Pt-deposited particles were almost the same as that of silica wall, as shown in Fig. 1. The direct observation of the particles has here been tried again by using a high resolution TEM at 1000 kV. Fig. 5 shows a typical TEM image of Fe/M41-12. The hexagonal arrays of M41's pores were clearly observed as white spots over the full range of the photograph. The diameter of pores and the wall thickness were 2.2 ± 0.2 and 1.2 ± 0.2 nm. The former value is in good agreement with that determined by the N_2 adsorption/desorption method. One can find that some of the pores became dark, some of which are indicated by black arrows in the figure. Since such dark spots could not be observed in the TEM images of the parent M41s, they might be attributed to iron oxide particles formed in the inside of the pores. The photograph indicates that the sizes of iron oxide particles are the same as the pore size of the M41-12 employed, indicating that the pores indeed act as the molds for the formation of nanoparticles of iron oxide.

3.3. Bandgaps of the iron oxide particles loaded in the pores

Fig. 6 shows UV-VIS absorption spectra of the Fe/supports, M41-12, and PVG-N, which were calculated by using Kubelka–Munk function ($F(R_\infty)$). The absorption spectrum of the bulk Fe_2O_3 sample is also depicted in the figure for comparison. The supports themselves, M41-12 and PVG-N, gave only small absorption peaks at 240–300 nm as described at Fig. 2 and the spectra of the other supports were very similar to those.

Three interesting phenomena could be pointed out in Fig. 6. First, the positions of absorption spectra were greatly shifted with the supports used. It will be discussed in the next section in more detail. Secondly, the slopes of the right-hand side of the respective spectra are all steep and almost constant on the Fe/supports samples. Taking the discussion described at Figs. 1 and 2 into consideration, the sharpness and the similarity of the UV-VIS adsorption edges conclude the uniform particle sizes of iron oxide on

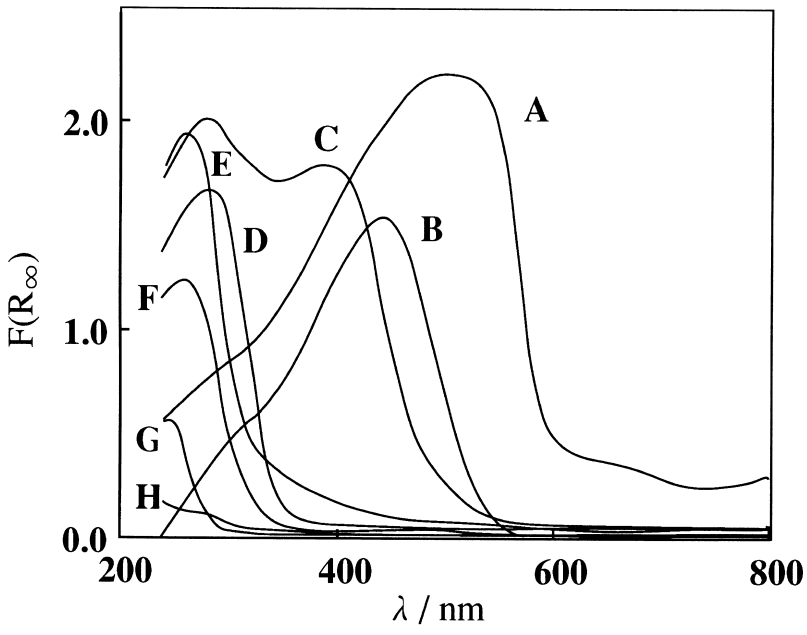

Fig. 6. Diffuse-reflectance UV-VIS spectra of (A) bulk Fe_2O_3, (B) Fe/PVG-N, (C) Fe/PVG-1263, (D) Fe/PVG-1273, (E) Fe/M41-16, (F) Fe/M41-12, (G) M41-12, and (H) PVG-N. The reference was $BaSO_4$.

the respective supports. Thirdly, there are two peaks at 300 and 410 nm in Fig. 6C. Formation of two kinds of nanoparticles or presence of two kinds of electron transition processes would be the reason for the phenomenon.

The absorption edge of an UV-VIS spectrum corresponds to the bandgap of the semiconductor and can be evaluated by the plot of $[F(R_\infty)h\nu]^2$ vs. $h\nu$ in the case of the direct interband transition [23]. The calculated bandgaps of the bulk Fe_2O_3 and the Fe/supports are summarized in Table 1. The values of the bulk Fe_2O_3 was 2.1 eV, which agreed well with the reported value of 2.2 eV [24,25]. In contrast, the bandgaps of the Fe/supports were greater than that of the bulk. The dependence of the bandgap on the pore size is plotted in Fig. 7, clearly showing that the bandgap increases with decreasing the pore size.

The size dependence of the bandgaps of several semiconductor particles, induced through a quantum size effect, has been discussed by a few researchers [26–29]. The tight-binding method has been successfully used to calculate the size-dependent bandgap of semiconductor particles [26]. In many case, however, it is necessary to use a lot of parameters to quantitatively determine the dependency; for example, 13 parameters have been used to give a satisfactory account of the bandgap of CdS samples. In the present study, we have employed a simpler equation based on the effective mass approximation, Brus' equation [1,2]. The bandgap energy of small particles (E) can be given by the following equations.

$$E = E_g + h^2\nu^2/d^2m - 1.8e^2/ed \quad (1)$$

$$1/m = (1/m_e + 1/m_h)/2 \quad (2)$$

In these equations E_g, e, and d are the bandgap of bulk semiconductor, its dielectric constant, and the radius of semiconductor particles, respectively. The m_e and m_h represent the effective masses of an electron and a hole in the bulk semiconductor. The solid line in Fig. 7 is the theoretical prediction calculated by using the

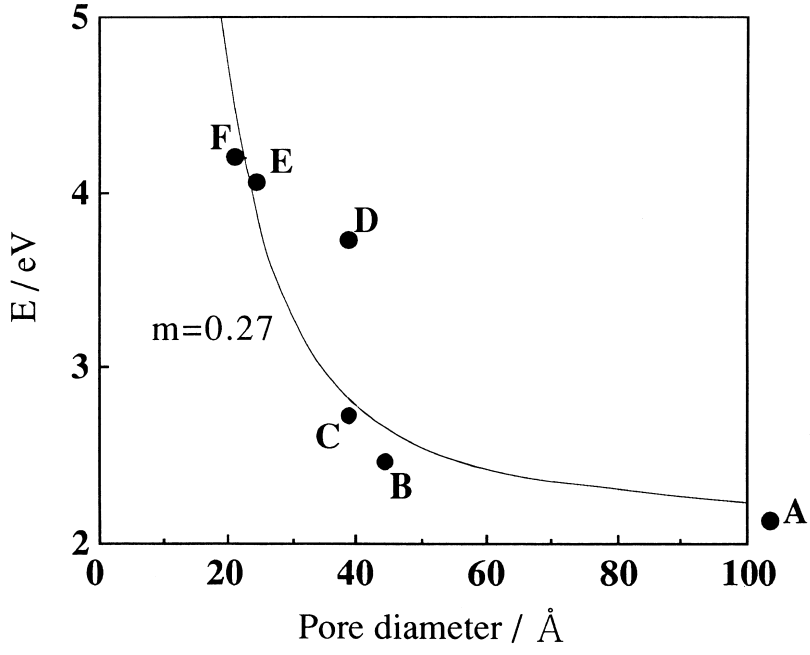

Fig. 7. Correlation of the observed bandgaps of iron oxide supported in various supports with the pore diameters of the supports: (A) Bulk Fe_2O_3, (B) Fe/PVG-N, (C) Fe/PVG-1263, (D) Fe/PVG-1273, (E) Fe/M41-16, and (F) Fe/M41-12. The solid line shows the theoretical calculation based on the Brus' equation with the effective mass of 0.27.

equations in which the average effective mass of an electron and a hole, *m*, was assumed to be 0.27. It is clear that all of the present data are well-plotted near the line. It follows that the supporting of iron oxide semiconductor particles into the nanometer-sized pores changed the bandgap of the resulting particles and the dependency of the bandgap on the pore size was attributable to the quantum size effect.

4. Conclusions

It was revealed that inorganic materials with uniform mesopores could be used for the molding of semiconductor oxide. The resultant nanometer-sized particles showed great change in the bandgap due to the quantum size effect. Although determining of the structure of iron oxide loaded was not carried out in the present study owing to the difficulties of use of the XRD technique, one can expect that the present method might be generalized to prepare uniform ultra-fine particles and also to control the bandgaps of semiconductors without any additives. In addition, high reactivity of the surface and new chemical and physical properties would be caused through this supporting treatment. The present value of the effective mass, 0.27, could not be compared with the data obtained by other method because no data was available on iron oxide at present. It should be noted that the value of the effective mass, 0.27, is comparable to the values of silicon, 0.19–0.92. The molding method reported here might be useful to determine the effective mass of semiconductor.

Acknowledgements

This work was partly supported by a Grant-in-aid for Scientific Research from the Ministry of Education, Science, Sports, and Culture of Japan.

References

[1] L.E. Brus, J. Chem. Phys. 80 (1984) 4403.
[2] R. Rossetti, R. Hull, J.M. Gibbon, L.E. Brus, J. Chem. Phys. 82 (1985) 552.
[3] N. Chestnoy, R. Hull, L.E. Brus, J. Chem. Phys. 85 (1986) 2237.
[4] E. Lifshitz, M. Yassen, L. Bykov, I. Dag, R. Chaim, J. Phys. Chem. 98 (1994) 1459.
[5] Y. Wang, A. Suna, W. Mahler, R. Kasowski, J. Chem. Phys. 87 (1987) 7315.
[6] N. Herron, Y. Wang, M.M. Eddy, G. Stucky, D.E. Cox, K. Moller, T. Bein, J. Am. Chem. Soc. 111 (1989) 530.
[7] M.E. Davis, R.F. Lobo, Chem. Mater. 4 (1992) 756.
[8] J.S. Beck, J.C. Vartuli, W.J. Roth, M.E. Leonowicz, C.T. Kresge, K.D. Schmitt, C.T.-W. Chu, D.H. Olson, E.W. Sheppard, S.B. McCulen, J.B. Higgins, J.L. Schlenker, J. Am. Chem. Soc. 114 (1992) 10834.
[9] A. Monnier, F. Schuth, Q. Huo, D. Kumar, D. Margolese, R.S. Maxwell, G.D. Stucky, M. Krishnamurty, P. Petroff, A. Firouzi, M. Janicke, B.F. Chmelka, Science 261 (1993) 1299.
[10] T. Yanagisawa, T. Shimizu, K. Kuroda, C. Katol, Bull. Chem. Soc. Jpn. 63 (1990) 988.
[11] M. Hartmann, A. Poppl, L. Kevan, J. Phys. Chem. 100 (1996) 9906.
[12] E.A. Gunnewegh, S.S. Gopie, H.V. Bekkum, J. Mol. Catal. A 106 (1996) 151.
[13] E. Armengol, M.L. Cano, A. Corma, H. Garcia, M.T. Navarro, J. Chem. Soc., Chem. Commun. (1995) 519.
[14] P.J. Branton, P.G. Hall, M. Treguer, S.W. Sing, J. Chem. Soc., Faraday Trans. 91 (1995) 2041.
[15] P.L. Llewellyn, F. Schuth, Y. Grillet, F. Rouquerol, J. Rouquerol, K.K. Unger, Langmuir 11 (1995) 574.
[16] A. Wu, T. Bein, Science 264 (1994) 1757.
[17] T. Abe, Y. Tachibana, T. Uematsu, M. Iwamoto, J. Chem. Soc., Chem. Commun. (1995) 1617.
[18] Y. Xu, C.H. Langford, J. Phys. Chem. B 101 (1997) 3115.
[19] V.I. Srdanov, I. Alexneit, G.D. Stucky, C.M. Reaves, S.P. DenBaars, J. Phys. Chem. B 102 (1998) 3341.
[20] J.R. Agger, M.W. Anderson, M.E. Pemble, O. Teransihi, Y. Nozue, J. Phys. Chem. B 102 (1998) 3345.
[21] D. Duonghong, E. Forgarello, M. Gratzel, J. Am. Chem. Soc. 103 (1981) 4685.
[22] S. Sato, J. Catal. 92 (1985) 11.
[23] A. Karcaly, I. Hevesi, Z. Naturforsch., A 26 (1971) 245.
[24] W.H. Strhlow, E.L. Cook, J. Phys. Chem. Ref. Data 2 (1973) 245.
[25] H. Miyoshi, H. Yoneyama, J. Chem. Soc., Faraday Trans. 1 85 (1989) 1873.
[26] Y. Wang, N. Herron, Phys. Rev. B 42 (1990) 7253.
[27] A.B. Murray, D.J. Norris, M.G. Bawendi, J. Am. Chem. Soc. I 15 (1993) 8706.
[28] A. Lifsshitz, M. Yassen, L. Bykov, I. Dag, R. Chaim, J. Phys. Chem. 98 (1994) 1459.
[29] H. Yoneyama, Electrochemistry 67 (1999) 324.